AKR-like emissions observed at low altitude by the DEMETER satellite

Michel Parrot, Jean-Jacques Berthelier

AKR-like emissions observed at low altitude by the DEMETER satellite

Michel Parrot[1] and Jean-Jacques Berthelier[2]

Received 15 May 2012; revised 29 August 2012; accepted 29 August 2012; published 11 October 2012.

[1] This paper reports observations of Auroral Kilometric Radiation (AKR) by the low altitude satellite DEMETER (700 km) during the super magnetic storm of November 2004. AKR is generated along auroral field lines at altitudes above ∼3000 km and escapes from the Earth so that most observations have been made close to the source regions or at large distances from the Earth. However, EM waves with AKR-like frequency spectra detected by the low altitude EXOS-C satellite were interpreted by Oya et al. (1985) as AKR emissions propagating toward the Earth in the whistler mode. During the large magnetic storm of November 8–10, 2004, numerous events have been observed by DEMETER and, in one case, the emissions were recorded when DEMETER was flying over an intense aurora observed by the UVI (Ultra Violet Imager) of the POLAR spacecraft. During this event, density depletions have been observed at the satellite altitude. Similar AKR-like EM waves were also recorded by DEMETER at other times showing that these emissions are a common phenomenon at low altitudes in the auroral regions during periods of sustained magnetic activity.

Citation: Parrot, M., and J.-J. Berthelier (2012), AKR-like emissions observed at low altitude by the DEMETER satellite, *J. Geophys. Res.*, *117*, A10314, doi:10.1029/2012JA017937.

1. Introduction

[2] Auroral Kilometric Radiation (AKR) is an electromagnetic emission generated by energetic electron beams precipitating along auroral magnetic field lines and cover the frequency range 50–700 kHz with a maximum around 250 kHz [*Gurnett*, 1974]. A detailed description of the most significant AKR features was given by *André* [1997] showing that the dominant mode of propagation is R-X, with a weaker L-O mode also observed. Z mode AKR can also be detected between the plasma frequency and the electron gyrofrequency [*Benson*, 1985; *Roux et al.*, 1993; *André*, 1997]. Using a ray tracing analysis, *Menietti and Lin* [1985] have shown that the Z mode propagates toward higher density regions, roughly perpendicularly to the Earth's magnetic field. AKR waves in the R-X mode propagate upwards and escape from the Earth because large scale density gradients refract the waves which are going downward. However, a few observations performed on-board low-altitude satellites have shown the existence of HF waves in the same frequency range but propagating in the whistler mode [*Hartz*, 1970; *Oya et al.*, 1985; *Benson and Wong*, 1987; *Beghin et al.*, 1989; *Kiraga*, 2010]. These findings have been discussed by *André* [1997] and *LaBelle and Treumann* [2002]. *Oya et al.* [1985] were the first to call them "AKR-like emissions" and to suggest a link with AKR. Recently, by comparison between AKR-like emissions observed on ground and AKR emissions observed by the GEOTAIL plasma wave receiver located very far from the Earth, *LaBelle and Anderson* [2011] found that the two emissions have the same frequency-time structure, and thus should have a common origin.

[3] This paper reports observations of AKR-like emissions recorded by the low altitude DEMETER satellite during the large magnetic storm of November 8–10, 2004. These observations were performed both in the northern and southern auroral regions. A particular event will be shown in more detail when DEMETER is just above an active auroral arc as evidenced by images from the UVI (Ultra Violet Imager) of the POLAR spacecraft. Section 2 describes the instrumentation, section 3 the observations and section 4 is devoted to discussion and conclusions.

2. Instrumentation

[4] DEMETER is a 3-axis stabilized Earth-pointing spacecraft launched on June 29, 2004 into a low altitude (∼710 km) polar and circular orbit that was subsequently lowered to 650 km till the end of the mission in December 2010 [*Cussac et al.*, 2006]. The orbit is nearly sun-synchronous with an ascending node at ∼22.30 LT in the night sector and a descending node at ∼10.30 LT during day-time early in the mission. The main objectives of DEMETER were the search for ionospheric disturbances possibly generated by pre-seismic activity, the investigation

[1]LPC2E, CNRS, Université d'Orléans, Orléans, France.
[2]LATMOS/IPSL, CNRS-UVSQ-UPMC, Saint-Maur des Fossés, France.

Corresponding author: M. Parrot, LPC2E, CNRS, 3A Ave. de la Recherche Scientifique, FR-45071, Orléans CEDEX 2, France. (mparrot@cnrs-orleans.fr)

0148-0227/12/2012JA017937

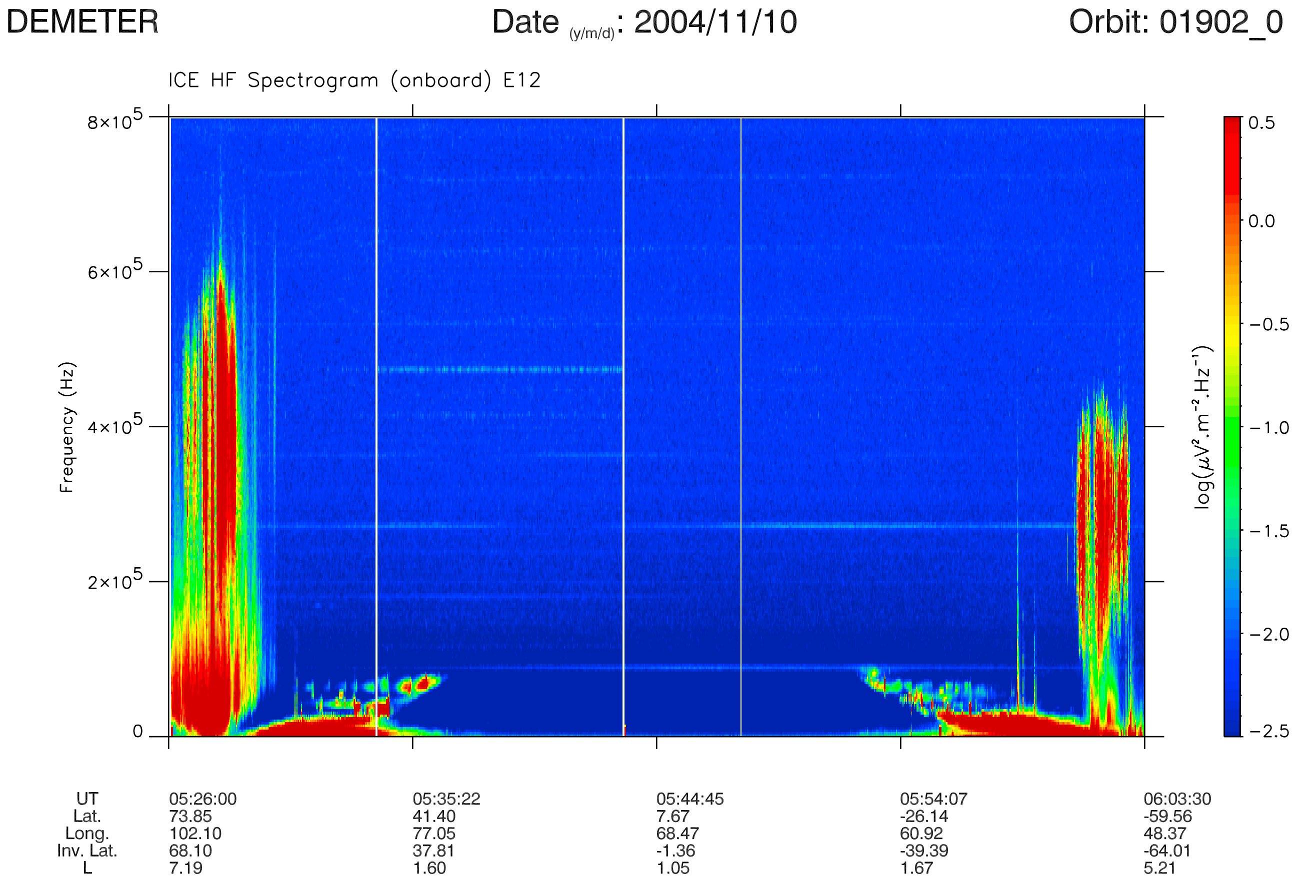

Figure 1. Electric HF spectrogram recorded on November 10, 2004 between 05:26:00 UT and 06:03:30 UT. The spectrogram is from 0 up to 800 kHz and its intensity is color coded according to the scale on the right. The parameters displayed below are the time in UT, the geographic latitude and longitude, the invariant latitude and the McIlwain parameter L.

of ionospheric effects of man-made activities and, more generally, the study of space weather and ionospheric phenomena. To these aims the scientific payload included a complete set of instruments to measure the electric and magnetic components of plasma waves and to monitor the main parameters of the ionospheric plasma. A thorough description of the instrumentation can be found in the *Planetary and Space Science* DEMETER Special Issue, 2006. The payload was nearly continuously operated at latitudes below 65° but dedicated operations were also programmed when the satellite was flying over ground-based facilities such as EISCAT or HAARP.

[5] Data reported in this paper were acquired by the Electric Field Instrument (ICE) which measures the 3 electric components of plasma waves in the frequency range from DC to 3.25 MHz and a detailed description can be found in *Berthelier et al.* [2006a]. The Very Low Frequency (VLF) range of ICE extends from 70 Hz to 20 kHz and the High-Frequency (HF) range from 10 kHz to 3.25 MHz. There are two scientific modes, Survey and Burst, this later being mainly activated when the satellite is above active seismic regions or for specific purposes. Only Survey mode data were available for this study providing the 2.048 s averaged VLF and HF power spectra of the electric component of plasma waves perpendicular to the orbit plane with a frequency resolution of 3.25 kHz in the HF range.

[6] The electron density is measured by the ISL Langmuir probe [*Lebreton et al.*, 2006] with a resolution of 1 s and the ion density and composition are provided by the IAP retarding potential analyzer [*Berthelier et al.*, 2006b] with a resolution of ~4 s in Survey modes.

[7] The Polar Spacecraft was launched on February 24, 1996 in a highly elliptical orbit, with apogee at 9 earth radii and perigee at 1.8 earth radii geocentric. The inclination is 86° and the period about 18 h. The Ultraviolet Imager (UVI) onboard POLAR consists of a camera and an electronic support package. The UVI is a two dimensional spatial imager which produces images of the Earth's auroral regions in the far ultraviolet wavelength range (130 nm to 190 nm). Details of the UVI experiment can be found in *Torr et al.* [1995].

3. Observations

[8] Figure 1 shows the HF spectrogram along a complete day-time half-orbit on November 10, 2004. Emissions in the AKR frequency range are detected both in the Northern and Southern high latitudes regions extending up to ~600 kHz in the North and ~400 kHz in the South. They appear to be more intense and over a wider latitudinal range in the North. At lower frequencies, in the VLF range, auroral hiss is

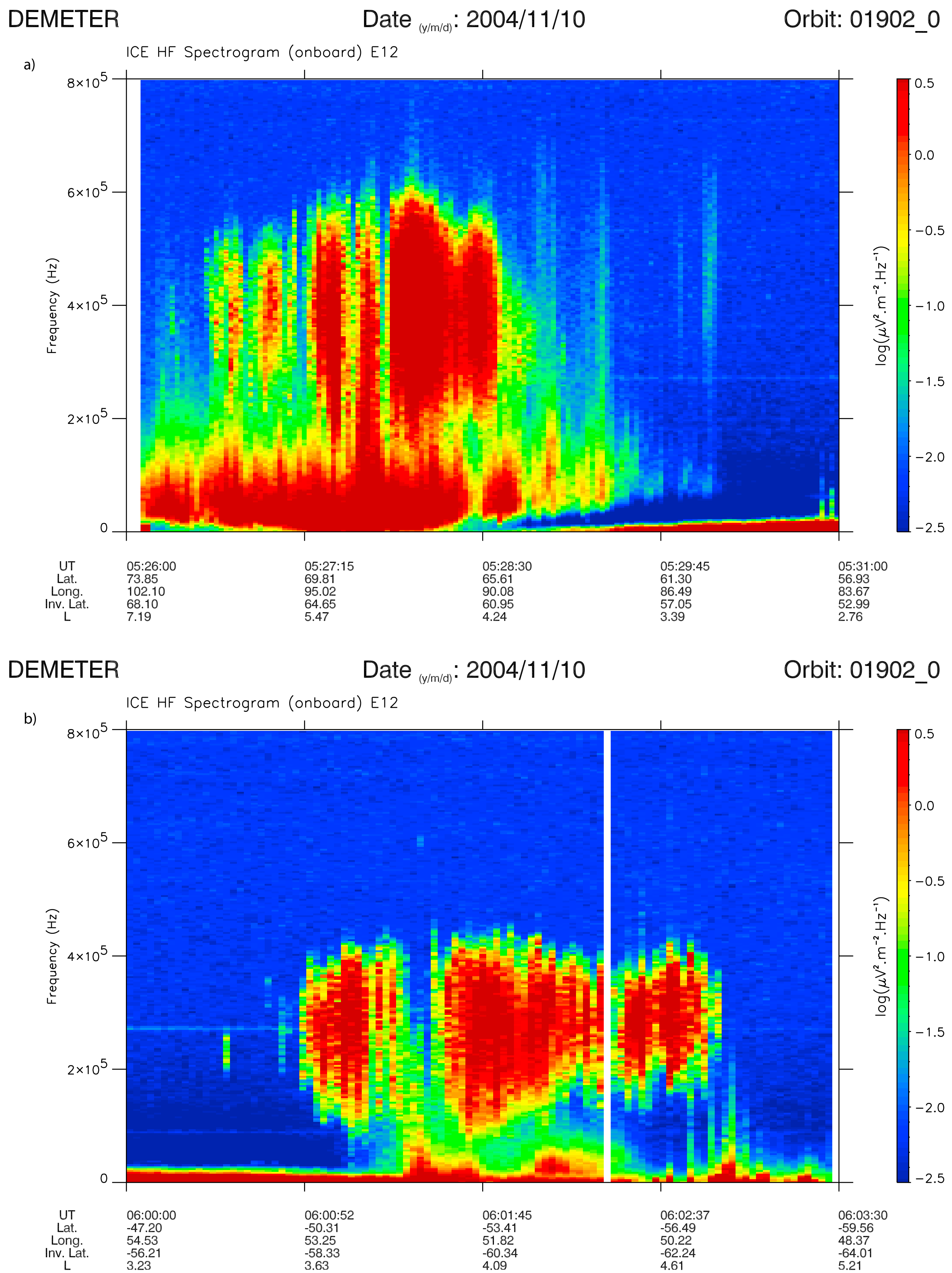
DEMETER
Date (y/m/d): 2004/11/10
Orbit: 01902_0
ICE HF Spectrogram (onboard) E12
a)
Frequency (Hz)
log(μV².m⁻².Hz⁻¹)
UT 05:26:00 05:27:15 05:28:30 05:29:45 05:31:00
Lat. 73.85 69.81 65.61 61.30 56.93
Long. 102.10 95.02 90.08 86.49 83.67
Inv. Lat. 68.10 64.65 60.95 57.05 52.99
L 7.19 5.47 4.24 3.39 2.76
DEMETER
Date (y/m/d): 2004/11/10
Orbit: 01902_0
ICE HF Spectrogram (onboard) E12
b)
Frequency (Hz)
log(μV².m⁻².Hz⁻¹)
UT 06:00:00 06:00:52 06:01:45 06:02:37 06:03:30
Lat. -47.20 -50.31 -53.41 -56.49 -59.56
Long. 54.53 53.25 51.82 50.22 48.37
Inv. Lat. -56.21 -58.33 -60.34 -62.24 -64.01
L 3.23 3.63 4.09 4.61 5.21

Figure 2

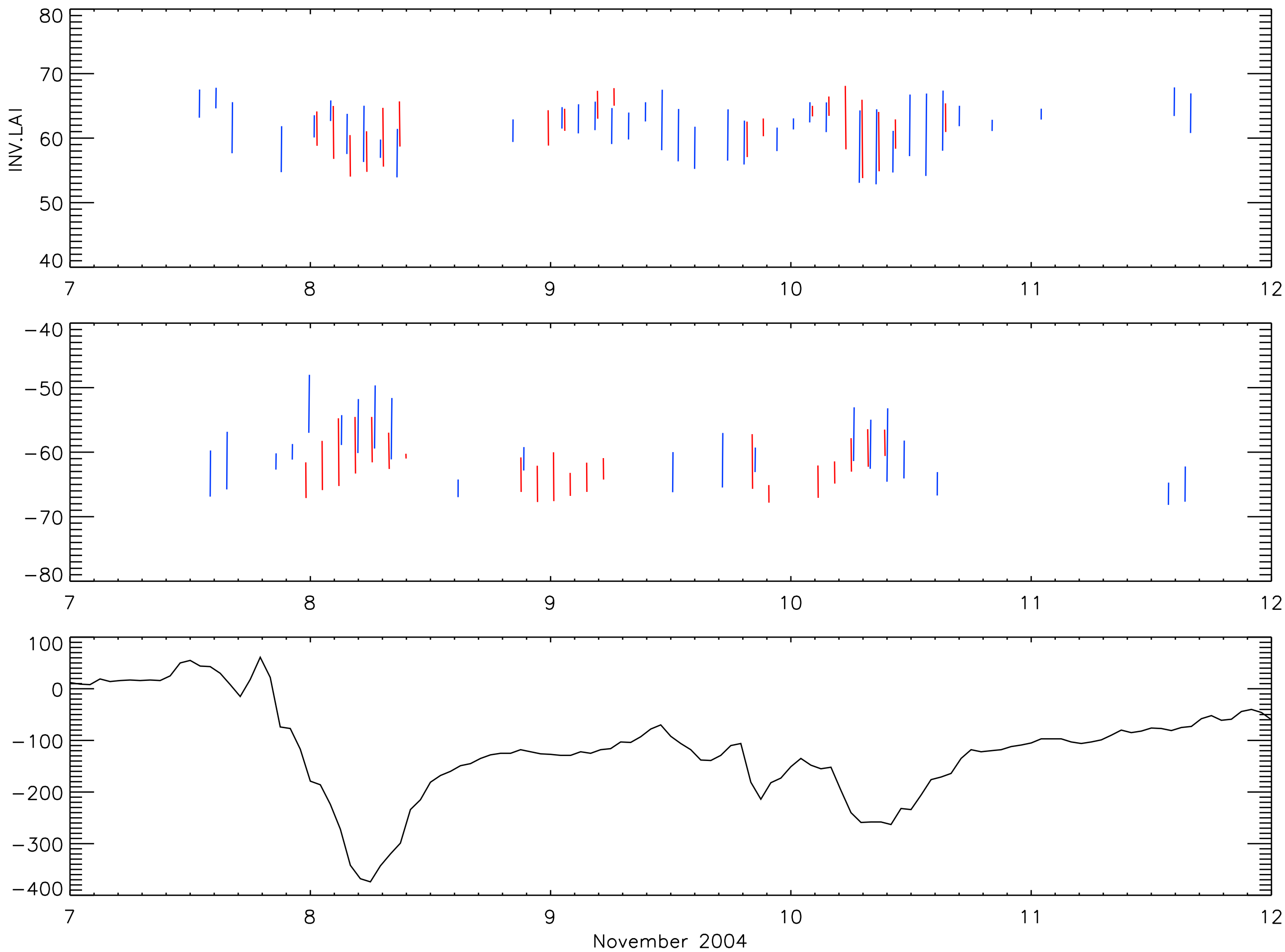

Figure 3. (top) The location in invariant latitude where DEMETER has observed AKR like emissions in the North hemisphere as function of days (from November 7 to November 11, 2004). (middle) As in Figure 3 (top), but for the South hemisphere. The day lines are in red whereas the night lines are in blue. (bottom) The Dst values during this November storm as function of days (data is from Kyoto WDC).

simultaneously observed. A zoom of Figure 1 is displayed in Figure 2 with Figures 2a and 2b corresponding to the Northern and Southern high latitude regions, respectively. In the North intense emissions are recorded over the frequency range from ∼200 to 600 kHz, from ∼05:26:30 to ∼05:29:00 UT encompassing the invariant latitude range from ∼66° to ∼61°. During the same period, the lower frequency cut-off of VLF emissions varies with latitude and its minimum value is roughly coincident with the center of the time interval where the AKR-like emissions are observed. Half an hour later, in the South part of the same half-orbit, HF emissions are recorded in a frequency range from 100 kHz to 400 kHz and between ∼06:00:40 UT and ∼06:02:50 UT corresponding to invariant latitudes from ∼−58° to −63° thus at invariant latitudes significantly lower than in the Northern hemisphere. Previous studies have shown that the patterns of auroral arcs and electron precipitations may be different in conjugate hemispheres [*Frey et al.*, 1999; *Østgaard et al.*, 2007]. An overview of AKR-like emissions detected during the whole period of the magnetic storm is displayed in Figures 3 and 4. Figure 3 (top) shows the invariant latitude intervals over which AKR-like emissions have been observed in the Northern hemisphere between November 7 and November 11, 2004, and Figure 3 (middle) displays the same results in the Southern hemisphere. Figure 3 (bottom) represents the variation of the Dst index during the same period. Figure 4 also displays, during the same 5 day period, the invariant latitude intervals where AKR-like emissions have been recorded but represented on a Magnetic Local Time (MLT)- Invariant Latitude map, Northern hemisphere data in Figure 4 (left) and Southern hemisphere data in Figure 4 (right). As noted in section 2, due the nearly fixed Local Time of the DEMETER orbits, the observations are only available in two MLT intervals of less than ∼2 h and are not indicative of the actual wider MLT distribution in both hemispheres. From Figures 3 and 4 it is clear that these

Figure 2. (a) Zoom of Figure 1 for the time interval between 05:26:00 UT and 05:31:00 UT. It corresponds to high latitudes in the North. (b) Zoom of Figure 1 for the time interval between 06:00:00 UT and 06:03:30 UT. It corresponds to high latitudes in the South.

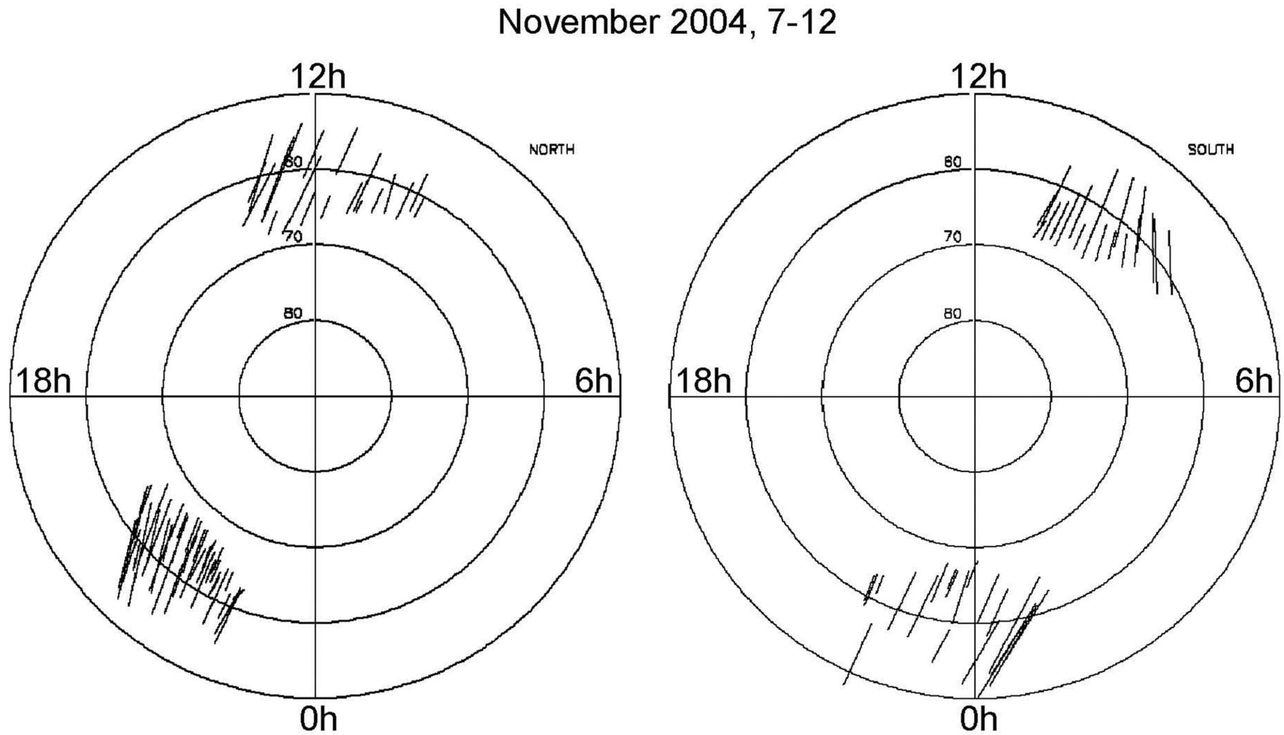

Figure 4. Same data as in Figure 3 but plotted as function of the invariant latitude and the Magnetic Local Time (MLT). Observations in the (left) North and (right) South hemisphere between November 7 and November 11, 2004.

AKR-like emissions are observed at auroral latitudes at night. Day-time emissions may occur along cusp/cleft field lines since AKR was also observed in this region [*Pottelette et al.*, 1990] which moves toward lower latitudes during periods of intense magnetic activity.

[9] A last example of AKR-like emissions is shown in Figure 5. The data were acquired in the Southern hemisphere during nighttime on November 8, 2004 between 06:24:30 and 06:30:30 UT. In addition to AKR-like signals at frequencies up to ~550 kHz, they show large signals extending up to ~1.35 MHz and, even, above 1.8 MHz over a short time interval near 06:27:15 UT which we discuss briefly later. This example is especially interesting because of the availability of a simultaneous UV image of the auroral oval obtained by the UVI experiment onboard POLAR exhibited in Figure 6. In Figure 6 (left), the image is in geographical coordinates and in Figure 6 (right), the image is displayed in magnetic latitudes and MLT coordinates with, indicated in red, the part of the DEMETER orbit during which AKR-like observations are performed. Clearly the emissions are detected when DEMETER flies over a relatively wide-spread auroral arc. Several UVI images similar to the one shown in Figure 6 are available showing that the aurora form is quite stable over a period of several minutes, thus during the period when AKR-like emissions are observed.

4. Discussion and Conclusions

[10] From a magnetic mapping, *Huff et al.* [1988] have shown that AKR sources occur on field lines associated with discrete auroral arcs and in situ measurements performed by VIKING [*Louarn et al.*, 1990] and FAST [*Ergun et al.*, 1998; *Pottelette et al.*, 2004] have shown that the source region typically extends from ~3000 km to 8000 km. However, *Benson and Calvert* [1979] have observed AKR sources down to 2000 km with ISIS-1 data. Using data from the same satellite, this minimum source region altitude for the source encounters is also confirmed in Figures 3–7 of *Benson and Akasofu* [1984] and Figures 27 and 28 of *Benson* [1985].

[11] The plots of Figure 6 indicate that AKR-like emissions are detected by DEMETER at low altitude along magnetic field lines connected to a visual auroral arc. Figure 7 is an extension of Figure 5 where Figure 7 (top) shows the spectrogram up to 3 MHz, Figure 7 (middle) displays the electron density, and Figure 7 (bottom) displays the ion density. Two density depletions are clearly seen at about 06:26:45 and 06:27:30 UT, corresponding in Figures 5 and 7 to strong enhancements of the ELF electrostatic turbulence and to HF signals up to the high frequency limit of the ICE experiment. Bursts of broadband waves in the HF frequency range in the auroral region have already been observed by other satellites (see the review by *LaBelle and Treumann* [2002]). They have been identified as electron beam driven upper hybrid emissions or as Broadband Electrostatic Noise (BEN) in AKR source regions at much higher altitudes [*Pottelette et al.*, 1988] shown to arise from electron holes moving along the field lines [*Dubouloz et al.*, 1991a, 1991b; *Berthomier et al.*, 2003]. However, due to instrumental effects in the ICE instrument HF channel in presence of large signals, we cannot rule out that these HF signals are of instrumental rather than natural origin. The

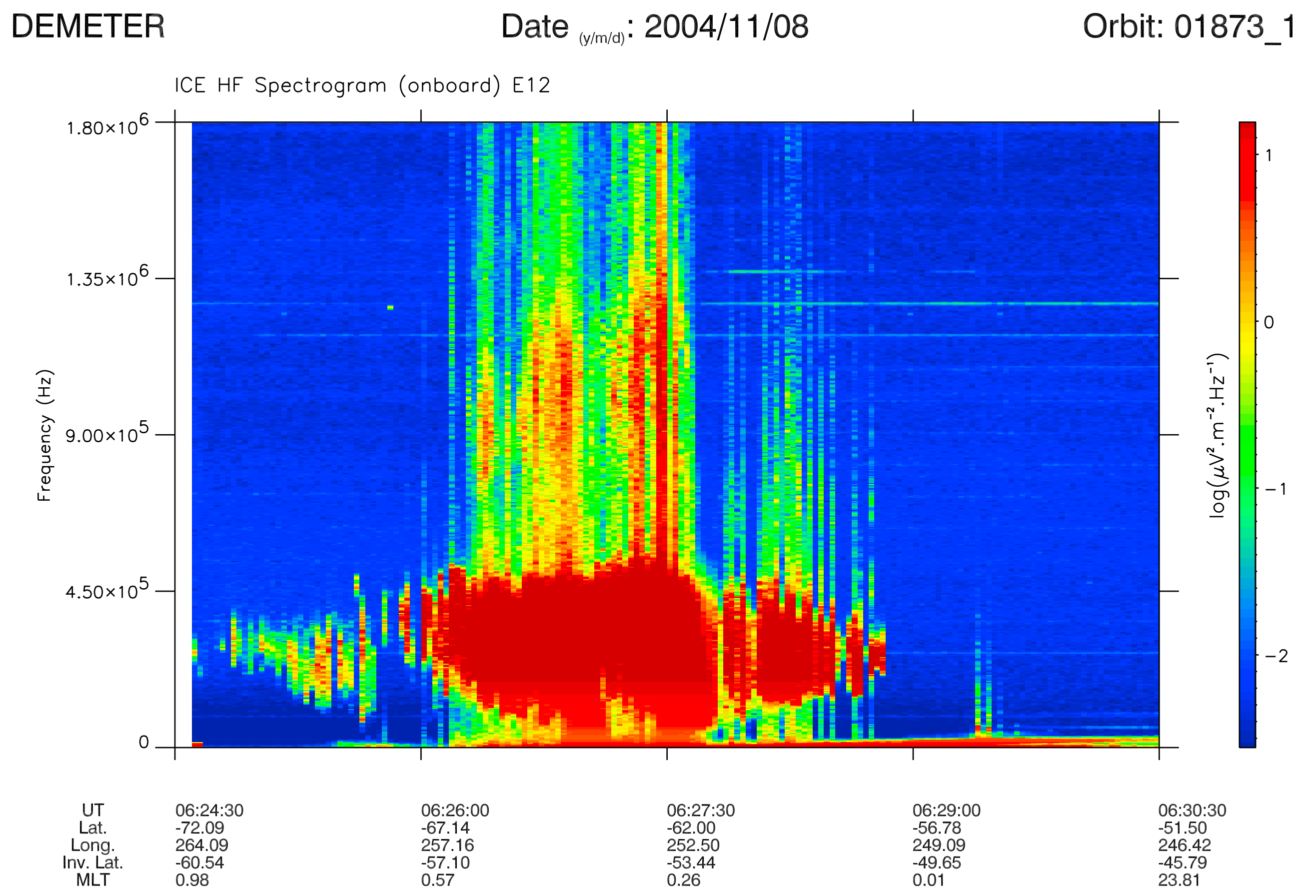

Figure 5. HF spectrogram of an electric component recorded on November 8, 2004 between 06:24:30 and 06:30:30 UT in the frequency range from 0 to 1.8 MHz.

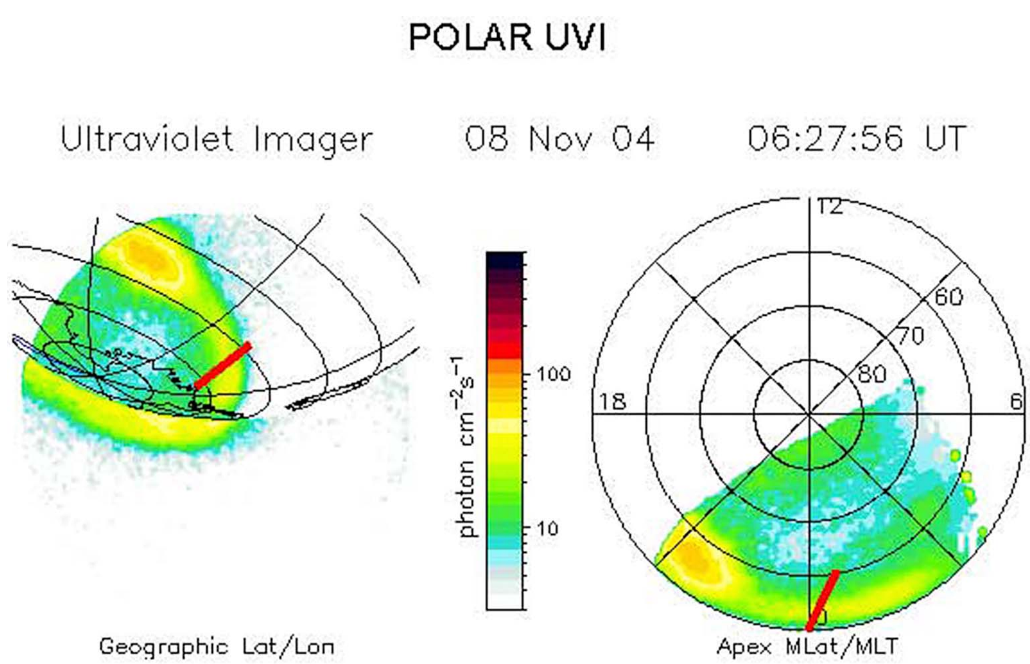

Figure 6. An UV image from the UVI experiment onboard POLAR at the same time as the DEMETER observation shown in Figure 5. The UV image is displayed (left) in geographic coordinates and (right) in magnetic latitude – MLT coordinates. On each side the red lines represent the trace of the DEMETER orbit when AKR-like emission is recorded.

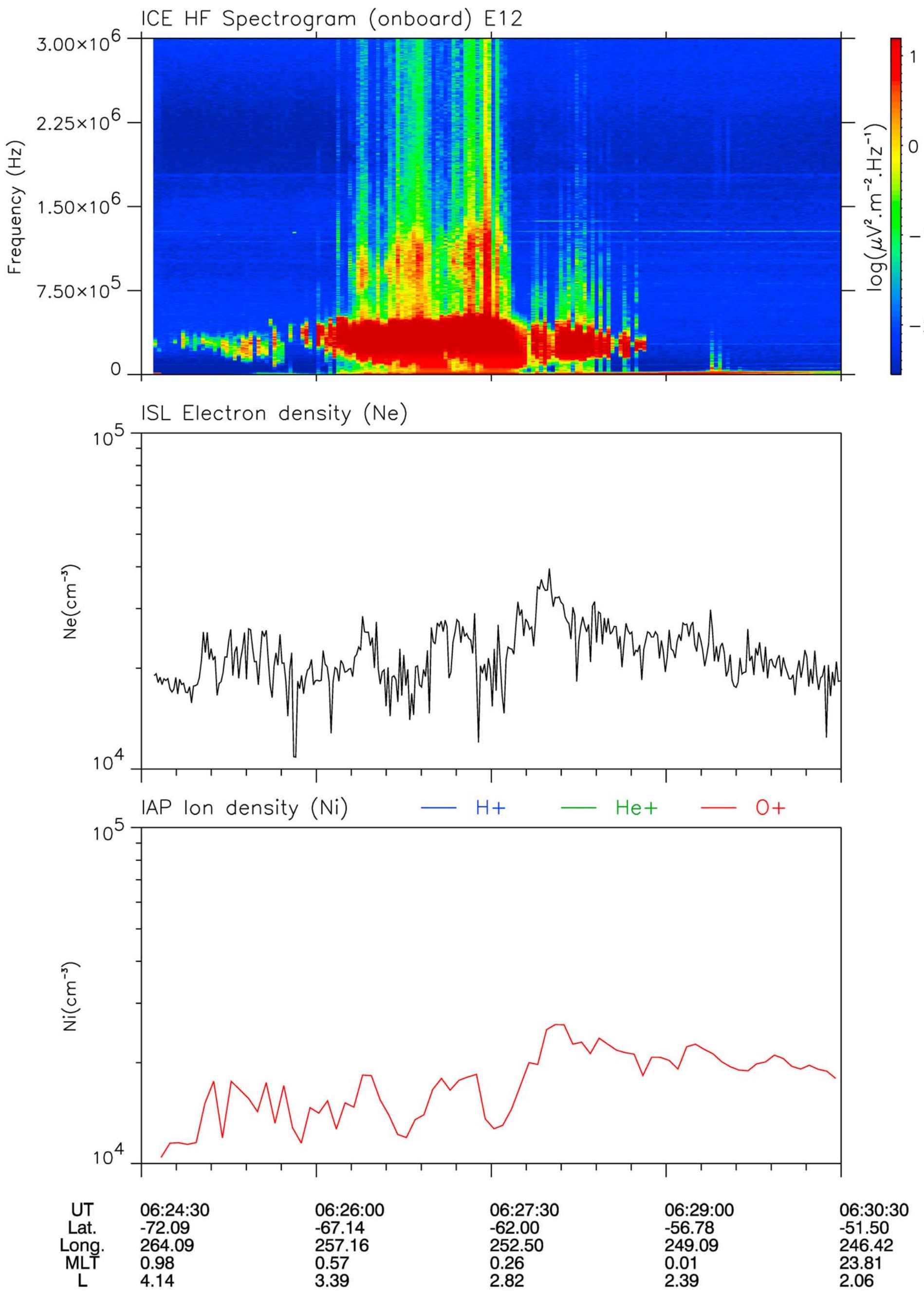

Figure 7. (top) The same spectrogram as in Figure 5 but up to 3 MHz the frequency limit of the experiment. (middle) The electron density obtained from ISL. (bottom) The ion density obtained from IAP. The parameters displayed below are the time in UT, the geographic latitude and longitude, the MLT and the McIlwain parameter L.

data are currently under investigation and the results will be reported in a forthcoming paper.

[12] There is no UVI POLAR data for the observations displayed in Figure 2a but the HF spectrogram of this event shown in Figure 8 displays similar features as those observed in conjunction with POLAR. Figure 8a presents the same HF spectrogram as in Figure 2 but now up to 200 kHz, and Figure 8b shows the VLF spectrogram from 70 Hz to 20 kHz. The ion and electron densities displayed in Figures 8c and 8d show the presence of a deep density depletion centered at ~05:27:45 UT with large fluctuations on the 1 s resolution electron density measurements and a simultaneous broadband electrostatic noise observed in the VLF spectrogram. It is likely that, once again for this event, the satellite crosses the field lines that link an auroral arc and the AKR source region. The latitudinal extension of the depletion region is about 110–200 km, very similar to the case of Figure 7 where the extension of each density cavity is of the order of 250 km. The DEMETER observations at 650 km altitude are thus very similar to observations

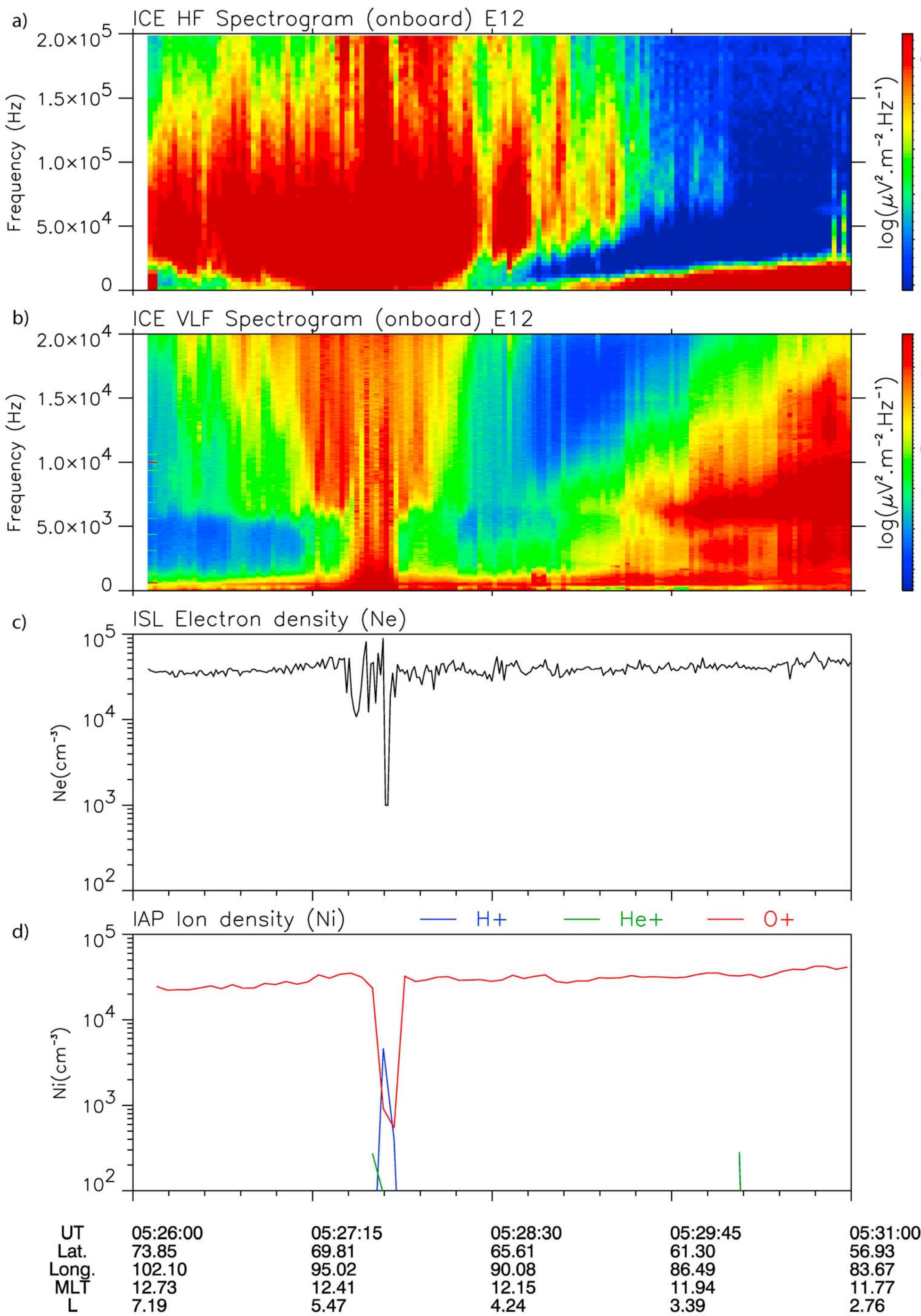

Figure 8. Data related to Figure 2a. (a) Low part of the HF spectrogram limited to 200 kHz, (b) VLF part of the spectrogram up to 20 kHz, (c) electron density given by ISL, and (d) ion density given by IAP (most of the time O+ is dominant except in the cavity where we have He+). The parameters displayed below are the time in UT, the geographic latitude and longitude, the MLT and the McIlwain parameter L.

obtained at much higher altitudes by FAST which show that the most intense AKR occurs in density depleted cavities extending from 30 km to 300 km in latitude [*Ergun et al.*, 1998]. Our data suggest that these density cavities are the signature of an AKR source region and extend along the magnetic field lines from the *F* region ionosphere connected to the visual auroral arc to the AKR source region at high altitude. To get some insight into the auroral electron precipitation at the time of an event, we have used the DC magnetic field measurements provided by the DEMETER service magnetometer that is part of the attitude and orbit control systems. In spite of the low sampling rate (1 point/s), low resolution (50 nT) and significant EM interferences due to S/C subsystems, this magnetometer provides useful data for intense auroral events. There is no magnetometer data for the two events previously shown in Figures 7 and 8, but

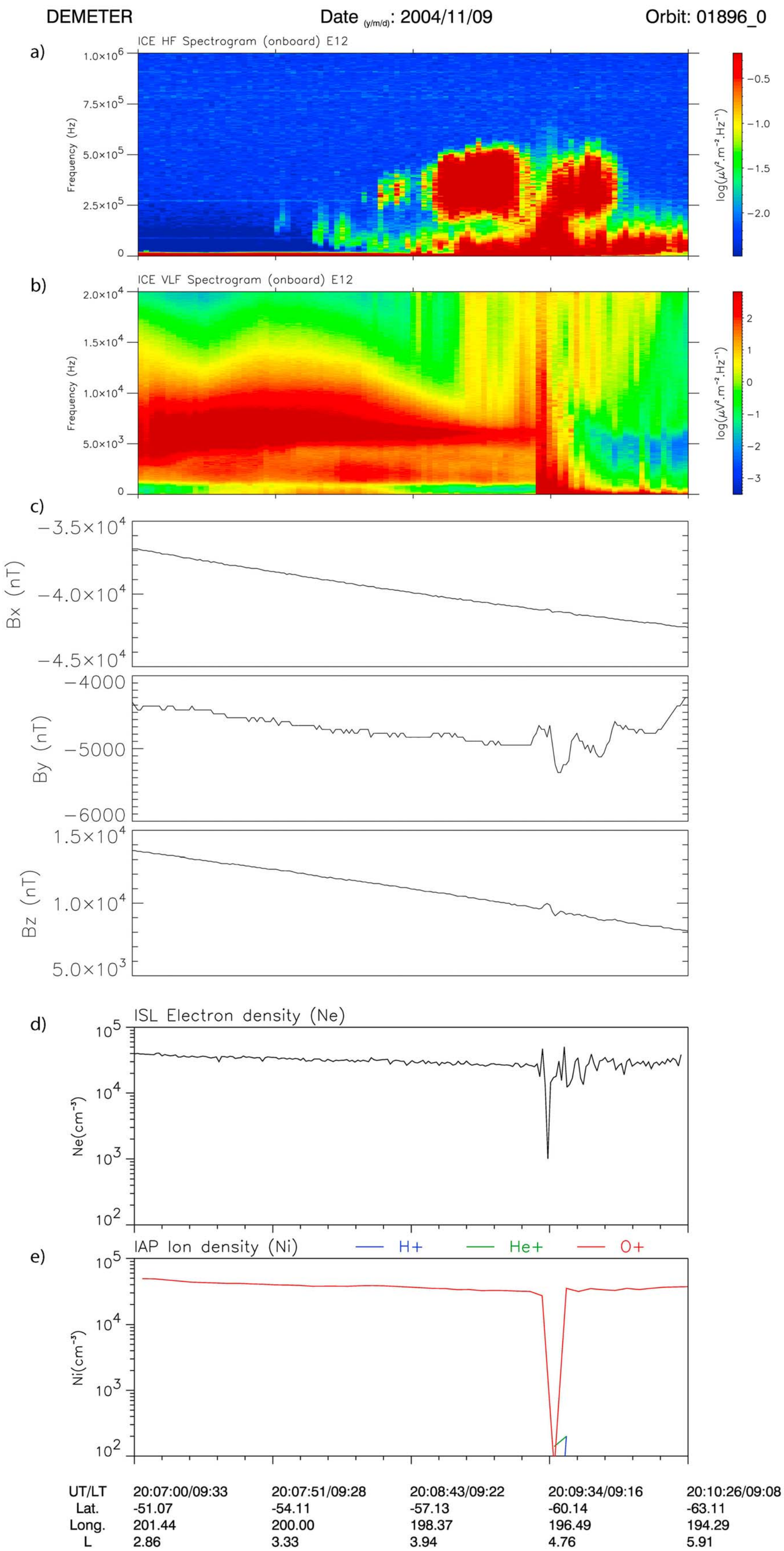
DEMETER
Date (y/m/d): 2004/11/09
Orbit: 01896_0
a)
ICE HF Spectrogram (onboard) E12
Frequency (Hz)
log(μV².m⁻².Hz⁻¹)
b)
ICE VLF Spectrogram (onboard) E12
c)
Bx (nT)
By (nT)
Bz (nT)
d)
ISL Electron density (Ne)
Ne(cm⁻³)
e)
IAP Ion density (Ni)
H+
He+
O+
Ni(cm⁻³)
UT/LT
Lat.
Long.
L
20:07:00/09:33
-51.07
201.44
2.86
20:07:51/09:28
-54.11
200.00
3.33
20:08:43/09:22
-57.13
198.37
3.94
20:09:34/09:16
-60.14
196.49
4.76
20:10:26/09:08
-63.11
194.29
5.91

Figure 9

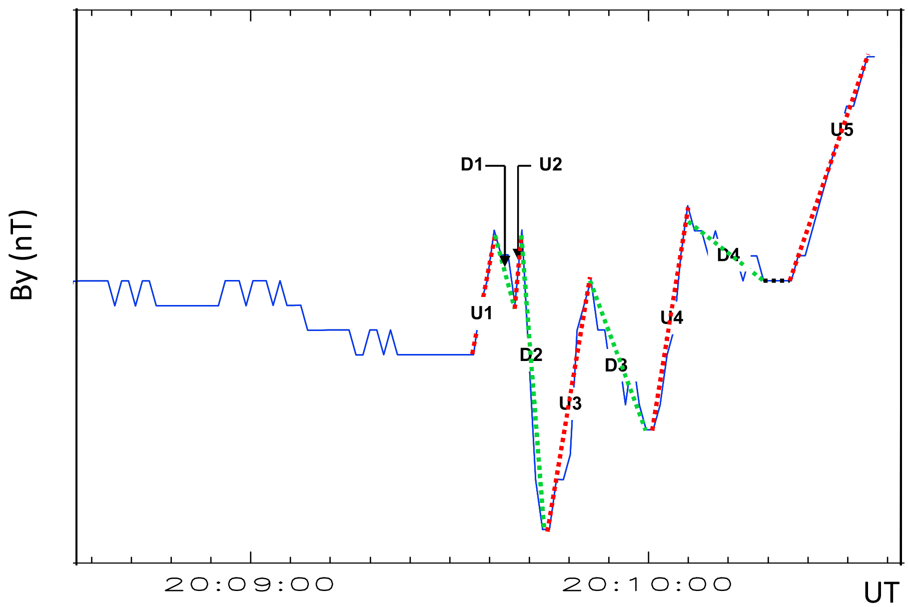

Figure 10. Zoom of the Y component of the magnetic field shown in Figure 9 with indication of the upward (U) and downward (D) current sheets.

another very similar case is displayed in Figure 9 where these data are available. In this figure the three magnetometer components are in the satellite coordinate system, i.e., Z is opposite to the satellite velocity, hence horizontal, X is directed toward the nadir and Y completes the orthogonal set. As usual, the major disturbances are observed on the Y component but smaller variations are also observed on the Z component indicating that the current sheets are inclined with respect to the perpendicular to the DEMETER orbit. Nevertheless, due to the relative amplitude of the Y and Z variations, and to the limited accuracy of the magnetometer data, we have calculated the current densities by taking only into account the Y component data which are displayed in a magnified scale in Figure 10. The field aligned currents are highly structured with successive alternated upwards (5) and downward (4) current sheets crossed between 20:09:33 UT and the end of the interval at 20:10:26 UT. The upward current densities range from $\sim$4 to $\sim$10 μA/m^2 with an average thickness of $\sim$50 km along the satellite track while the downward current densities range from ~ -1 to -12.5 μA/m^2. The current densities maximize at $\sim$+10 and ~ -12.5 μA/m^2 in a pair of upward and downward current sheets observed between $\sim$20:09:40 and 20:09:44.4 UT with respective thicknesses of $\sim$8 km and $\sim$25 km. The most intense upward field aligned current is thus observed in a $\sim$8 km sheet between 20:09:40 and 20:09:41 UT which can be associated with the plasma cavity observed at $\sim$20:09:39 UT by the plasma instruments. This is in accordance with the expectation that AKR emissions are generated by precipitating electron beams.

[13] The spectrograms in Figures 1, 2 and 5 similarly show frequency ranges comparable to the usual AKR frequency band. Unfortunately the reduced capability of the HF part of the ICE experiment with a single component on a non-spinning spacecraft does not allow performing a more thorough analysis of the emissions, in particular determining the wave polarization and the propagation direction. For the events shown in Figures 1, 2 and 5, electron density measurements correspond to a local plasma frequency between 1.3 MHz and 1.8 MHz while the computed gyrofrequency is between 1.0 and 1.2 MHz. Thus it is likely that the detected waves propagate in the whistler mode. Our observations thus relates to those performed by *Oya et al.* [1985] who concluded that these AKR-like emissions are leaked AKR. They develop a theoretical interpretation showing that Z-mode waves generated in the source region well above the satellite altitude are partly converted to the whistler mode waves at the point where the Z-mode wave frequency coincides with the local plasma frequency. Later on, *Horne* [1995] using a ray tracing analysis has shown that Z-mode waves are reflected in the topside of the ionosphere at an altitude of $\sim$1.1 R_E (in fact very close to the DEMETER altitude). But he also demonstrated that the Z-mode waves can access to the so-called second radio window [*Jones*, 1976] where energy can be mode converted into whistler mode waves which propagate to the ground. It can therefore be concluded that the observed HF waves are AKR emissions which propagate with large enough amplitudes down to the upper *F* region at DEMETER altitude.

[14] During the time interval of observations in Figures 3 and 4, some half orbits are missing due to the satellite

Figure 9. Data recorded on November 9, 2004 between 02:07:00 and 02:10:26 UT. (a) The low part of the HF spectrogram limited to 1 MHz, (b) the VLF part of the spectrogram up to 20 kHz, (c) the three components of the DC magnetic field, (d) the electron density given by ISL, and (e) the ion density given by IAP. The parameters displayed below are the time in UT/LT, the geographic latitude and longitude, and the McIlwain parameter L.

operation but it is shown that AKR-like emissions are always present during this super magnetic storm. They are detected in the nighttime auroral zone as well as in day-time where they most probably relate to a source in the cusp/cleft region. Such AKR-like emissions are not only observed by DEMETER during the November 2004 storm but also each time the magnetosphere is compressed enough that the auroral oval is present at invariant latitude less than 65° where DEMETER data are usually recorded or in the few high latitude DEMETER passes dedicated to correlated studies with HAARP and EISCAT. This indicates that these AKR emissions are a common phenomenon at high latitudes and low altitudes.

[15] **Acknowledgments.** This work was supported by continuous funding by CNES during the DEMETER mission analysis phase. The authors thank G. K. Parks the PI of the UVI experiment onboard POLAR and J. P. Lebreton, PI of the ISL experiment onboard DEMETER for the use of electron density data. They also wish to thank one referee for pointing out possible instrumental effects that need to be corrected for a proper interpretation of the data. J.J.B. acknowledges useful discussions with R. Pottelette.

[16] Robert Lysak thanks Robert Benson and another reviewer for their assistance in evaluating this paper.

References

André, M. (1997), Waves and wave-particle interactions in the auroral region, *J. Atmos. Sol. Terr. Phys.*, *59*(14), 1687–1712, doi:10.1016/S1364-6826(96)00173-3.

Beghin, C., J. L. Rauch, and J. M. Bosqued (1989), Electrostatic plasma waves and HF auroral hiss generated at low altitude, *J. Geophys. Res.*, *94*(A2), 1359–1378, doi:10.1029/JA094iA02p01359.

Benson, R. F. (1985), Auroral kilometric radiation: Wave modes, harmonics, and source region electron density structures, *J. Geophys. Res.*, *90*(A3), 2753–2784, doi:10.1029/JA090iA03p02753.

Benson, R. F., and S.-I. Akasofu (1984), Auroral kilometric radiation/aurora correlation, *Radio Sci.*, *19*(2), 527–541, doi:10.1029/RS019i002p00527.

Benson, R. F., and W. Calvert (1979), ISIS 1 observations at the source of auroral kilometric radiation, *Geophys. Res. Lett.*, *6*(6), 479–482, doi:10.1029/GL006i006p00479.

Benson, R. F., and H. K. Wong (1987), Low-altitude ISIS 1 observations of auroral radio emissions and their significance to the cyclotron maser instability, *J. Geophys. Res.*, *92*(A2), 1218–1230, doi:10.1029/JA092iA02p01218.

Berthelier, J. J., et al. (2006a), ICE, the electric field experiment on DEMETER, *Planet. Space Sci.*, *54*, 456–471, doi:10.1016/j.pss.2005.10.016.

Berthelier, J. J., M. Godefroy, F. Leblanc, E. Seran, D. Peschard, P. Gilbert, and J. Artru (2006b), IAP, the thermal plasma analyzer on DEMETER, *Planet. Space Sci.*, *54*, 487–501, doi:10.1016/j.pss.2005.10.018.

Berthomier, M., R. Pottelette, L. Muschietti, I. Roth, and C. W. Carlson (2003), Scaling of 3D solitary waves observed by FAST and POLAR, *Geophys. Res. Lett.*, *30*(22), 2148, doi:10.1029/2003GL018491.

Cussac, T., et al. (2006), The DEMETER microsatellite and ground segment, *Planet. Space Sci.*, *54*, 413–427, doi:10.1016/j.pss.2005.10.013.

Dubouloz, N., R. Pottelette, M. Malingre, and R. A. Treumann (1991a), Generation of broadband electrostatic noise by electron acoustic solitons, *Geophys. Res. Lett.*, *18*(2), 155–158, doi:10.1029/90GL02677.

Dubouloz, N., R. Pottelette, M. Malingre, G. Holmgren, and P. A. Lindqvist (1991b), Detailed analysis of broadband electrostatic noise in the dayside auroral zone, *J. Geophys. Res.*, *96*(A3), 3565–3579, doi:10.1029/90JA02355.

Ergun, R. E., et al. (1998), FAST satellite wave observations in the AKR source region, *Geophys. Res. Lett.*, *25*(12), 2061–2064, doi:10.1029/98GL00570.

Frey, H. U., S. B. Mende, H. B. Vo, M. Brittnacher, and G. K. Parks (1999), Conjugate observation of optical aurora with polar satellite and ground-based cameras, *Adv. Space Res.*, *23*(10), 1647–1652, doi:10.1016/S0273-1177(99)00379-8.

Gurnett, D. A. (1974), The Earth as a radio source: Terrestrial kilometric radiation, *J. Geophys. Res.*, *79*(28), 4227–4238, doi:10.1029/JA079i028p04227.

Hartz, T. (1970), Low frequency noise emissions and their significance for energetic particle processes in the polar magnetosphere, in *The Polar Ionosphere and Magnetospheric Processes*, edited by G. Skouli, pp. 151–160, Gordon and Breach, New York.

Horne, R. B. (1995), Propagation to the ground at high latitudes of auroral radio noise below the electron gyrofrequency, *J. Geophys. Res.*, *100*(A8), 14,637–14,645, doi:10.1029/95JA00633.

Huff, R. L., W. Calvert, J. D. Craven, L. A. Frank, and D. A. Gurnett (1988), Mapping of auroral kilometric radiation sources to the aurora, *J. Geophys. Res.*, *93*(A10), 11,445–11,454, doi:10.1029/JA093iA10p11445.

Jones, D. (1976), The second Z-propagation window, *Nature*, *262*, 674–675, doi:10.1038/262674a0.

Kiraga, A., (2010), An investigation of high frequency auroral plasma emissions with a tubular dipole antenna, *Adv. Space Res.*, *45*(4), 553–575, doi:10.1016/j.asr.2009.08.028.

LaBelle, J., and R. R. Anderson (2011), Ground-level detection of auroral kilometric radiation, *Geophys. Res. Lett.*, *38*, L04104, doi:10.1029/2010GL046411.

LaBelle, J. W., and R. A. Treumann (2002), Auroral radio emissions, 1. hisses, roars, and bursts, *Space Sci. Rev.*, *101*, 295–440, doi:10.1023/A:1020850022070.

Lebreton, J. P., et al. (2006), The ISL Langmuir probe experiment and its data processing onboard DEMETER: Scientific objectives, description and first results, *Planet. Space Sci.*, *54*, 472–486, doi:10.1016/j.pss.2005.10.017.

Louarn, P., A. Roux, H. de Feraudy, D. Le Quéau, A. André, and L. Matson (1990), Trapped electrons as a free energy source for the auroral kilometric radiation, *J. Geophys. Res.*, *95*(A5), 5983–5995, doi:10.1029/JA095iA05p05983.

Menietti, J. D., and C. S. Lin (1985), Ray tracing of Z-mode emissions from source regions in the high-altitude auroral zone, *Geophys. Res. Lett.*, *12*(6), 385–388, doi:10.1029/GL012i006p00385.

Østgaard, N., S. B. Mende, H. U. Frey, J. B. Sigwarth, A. Åsnes, and J. M. Weygand (2007), Auroral conjugacy studies based on global imaging, *J. Atmos. Sol. Terr. Phys.*, *69*(3), 249–255, doi:10.1016/j.jastp.2006.05.026.

Oya, H., A. Morioka, and T. Obara (1985), Leaked AKR and terrestrial hectometric radiations discovered by the plasma wave and sounder experiments on the EXOS-C satellite—Instrumentation and observation results of plasma wave phenomena, *J. Geomagn. Geoelectr.*, *37*, 237–262, doi:10.5636/jgg.37.237.

Pottelette, R., M. Malingre, A. Bahnsen, L. Eliasson, K. Stasiewicz, R. E. Erlandson, and G. E. Marklund (1988), VIKING observations of burst of intense broadband noise in the source regions of auroral kilometric radiation, *Ann. Geophys.*, *6*(5), 573–586.

Pottelette, R., M. Malingre, N. Dubouloz, B. Aparicio, G. Holmgren, and G. Marklund (1990), High frequency waves in the cusp/cleft regions, *J. Geophys. Res.*, *95*(A5), 5957–5971, doi:10.1029/JA095iA05p05957.

Pottelette, R., R. A. Treumann, and E. Georgescu (2004), Crossing a narrow-in-altitude turbulent auroral acceleration region, *Nonlinear Process. Geophys.*, *11*, 197–204, doi:10.5194/npg-11-197-2004.

Roux, A., A. Hilgers, H. de Feraudy, P. Louarn, S. Perraut, A. Bahnsen, M. Jespersen, E. Ungstrup, and M. André (1993), Auroral kilometric radiation sources: In situ and remote observations from Viking, *J. Geophys. Res.*, *98*(A7), 11,657–11,670, doi:10.1029/92JA02309.

Torr, M. R., et al. (1995), A Far Ultraviolet Imager for the International Solar Terrestrial Physics Mission, *Space Sci. Rev.*, *71*, 329–383, doi:10.1007/BF00751335.